RSC Advances

ROYAL SOCIETY OF CHEMISTRY

www.rsc.org/advances

Preparation of core-shell attapulgite particles by redox-initiated surface reversible addition-fragmentation chain transfer polymerization via "graft from" approach

Haicun Yang,[†] Sheng Xue,[§] Ji Pan,[§] Fanghong Gong,[*,‡,§] and Hongting Pu[*,†]

ABSTRACT: Nanoclay attapulgite (ATP) was first activated with hydrochloric acid to enhance the surface reactivity, and was then allowed to react with a synthetic aromatic tertiary amine coupling agent to introduce electron-donor groups. Subsequently, the surface-initiated reversible addition-fragmentation chain transfer (SI-RAFT) polymerization of methyl methacrylate (MMA) was carried out in presence of free RAFT agent cyanoisopropyl dithiobenzoate (CPDB) initiated by a redox pair made up of benzoyl peroxide (BPO) and aromatic tertiary amine functionalized ATP (ATP-ATA). The grafting process was verified by ^{1}H nuclear magnetic resonance, UV-visible spectroscopy, Fourier transform infrared spectroscopy, X-ray photoelectron spectroscopy, X-ray diffraction, Thermo gravimetric analysis, Transmission electron microscopy and Gel permeation chromatography. Kinetic behavior indicated that polymerization using this redox initiation system displayed the living/controlled nature. Both the grafted and free polymers were grown in a controlled manner, and the RAFT polymerization proceeded with 37.6% monomer conversion achieved within 10 h at 50 °C, yielding about 47.4% grafting ratio of

[†]*School of Materials Science and Engineering, Tongji University, Shanghai, 201804, China*
[‡] *School of Mechanical Technology, Wuxi Institute of Technology, Wuxi, Jiangsu 214121, China*
[§]*School of Materials Science and Engineering, Changzhou University, Changzhou, Jiangsu 213164, China*
[*]*Correspondence to: Hongting Pu (E-mail: puhongting@tongji.edu.cn) or Fanghong Gong (E-mail: fhgong@cczu.edu.cn)*

polymer relative to hybrid particles with high affinity to organic media.

KEYWORDS: attapulgite, surface-initiated RAFT polymerization, redox initiation system, surface modification, kinetic behavior

Introduction

Attapulgite (ATP) clay mineral has a typical unit cell consisting of [(Mg, $Al)_4(Si)_8(O,OH,H_2O)_{26}\cdot nH_2O$], which was illustrated by Bradley early in 1940.[1] ATP is a hydrated magnesium aluminum silicate in appearance with the diameter of a single rod less than 50 nm. The strong Van der Waals attraction force results in the formation of large compact bundles.[2] Nevertheless, this multifunctional nanoclay has played an important role in agriculture, sorbing materials and industrial catalysis.[3-5] In recent decades, the thermal stability and excellent mechanical strength of ATP are very attractive in preparation of polymer/ATP nanocomposites.[6-10] However, aggregation of ATP is a tough problem which needs to be dissolved. Functionalization of ATP is expected to be the promising approach to further exploiting its application in polymer nanocomposites.[11] The surface-grafted macromolecules can increase the surface wettability and dispersion of particulates in organic solvent.[12,13]

Generally, the surface-grafted polymer chains can be introduced by "grafting onto" or "grafting from".[14] "Grafting to", where already synthesized polymer chains characterized by appropriate functional groups, interact with particles surface to introduce anchoring chains.[15,16] Considering the diffusion ability of grafting units, the number of polymer chains per surface area can be significantly higher when "grafting

from" is employed.[17,18] In terms of surface-initiated controlled/living polymerization, the visible advantage of "grafting from" strategy is the ability to design and control the molecular weight coupled with a high degree of flexibility towards different chain growth mechanisms.[19] A variety of living polymerization, including cationic, anionic, group transfer and controlled radical polymerization (CRPs) have been used to graft polymer on to the surface of different inorganic particles.[20-23] Among those different CRPs, reversible addition-fragmentation chain transfer polymerization (RAFT) has shown the compatibility with functional monomer and the immunity to transition metal ion contamination as compared with nitroxide-mediated polymerization (NMP) and atom transfer radical polymerization (ATRP).[24-26] Up to date, RAFT technique has been widely applied on the surface modification of solid such as gold nanoparticles, carbon nanotubes, silica, cellulose and stainless steel.[27-32] As for ATP, however, the related reports are comparatively scarce. For example, Wang et al. prepared PMMA brushes on ATP surface by using benzyl dithiopropyltrimethoxysilane functionalized ATP as a RAFT chain transfer agent.[33] In summary, RAFT agent can be attached either via Z-group or R-group, and each method has its advantage and disadvantage.[34] Additionally, using a surface-anchored azo initiator and free RAFT agent in solution has also been reported previously.[35,36]

As is well known, conducting living free radical polymerization at lower temperature by using appropriate initiator is clearly a desirable feature with both academic and industrial standpoint.[37] Zheng and Sanchez-Sanchez reported a room temperature RAFT polymerization via redox initiator made up of benzoyl peroxide

(BPO) and N,N-dimethylaniline (DMA).[38,39] Then, Bai et al. carried out room temperature RAFT polymerization of N-isopropylacrylamide (NIPAM) and acrylamide (AM) by using potassium persulfate ($K_2S_2O_8$) and sodium thiosulfate ($Na_2S_2O_3$) as the aqueous redox initiator.[40] Enlightened by the aforementioned summary, in the present work, we report a facile and moderate surface-initiated RAFT (SI-RAFT) polymerization initiated by a redox pair consisting of BPO and aromatic tertiary amine functionalized ATP (ATP-ATA) in presence of free RAFT agent. The grafting procedure is characterized in detail, and the kinetics is investigated. It is worth noting that the complex process to attach conventional initiator or RAFT agent can be avoided by this approach.

Experimental section

Materials

Attapulgite (ATP,) was supplied by Jiangsu Jiuchuan Nano-material Technology Co. (Jiangsu, China). 3-aminopropyltriethoxysilane (APTES, 98%) and *p*-toluenesulfonic acid (PTSA, AR) were purchased from Aladdin-reagent Co. (Shanghai, China), PTSA was purified by recrystallization from toluene. 4-(diethylamino) salicylaldehyde (DEAS, 99%) was provided by Chengdu Xiya Chemical Technology Co. (Sichuan, China). Methyl methacrylate (MMA, AR) and benzoyl peroxide (BPO, CP) were obtained from Sinopharm Chemical Reagent Co. (Shanghai, China), MMA was passed through column of basic alumina to remove inhibitors, and then distilled under reduced pressure. BPO was purified by recrystallization from chloroform. Cyanopropyl dithiobenzoate (CPDB) was

synthesized according to the literature reported previously.[41] Toluene (AR) and methoxybenzene (AR) were obtained from Sinopharm Chemical Reagent (Shanghai, China) and used after dehydration. All other organic solvents were of analytical grade and used as received.

Synthesis of aromatic tertiary amine silane coupling agent

The aromatic tertiary amine coupling agent (SCA-ATA) was synthesized via aldehydic-amide condensation according to the method we have reported previously.[42] ^{1}H NMR (400 MHz, δ, ppm, $CDCl_3$): 7.91 (1H, s, -N=CH-), 6.94-6.96 (1H, d, ArH), 6.12-6.14 (1H, d, ArH), 6.04 (1H, s, ArH), 3.79-3.83 (6H, t, $-CH_2-$), 3.41-3.48 (2H, t, $-CH_2-$), 3.33-3.38 (4H, t, $-CH_2-$), 1.73-1.80 (2H, t, $-CH_2-$), 1.19-1.24 (9H, t, $-CH_3$), 1.15-1.18 (6H, t, $-CH_3$), 0.65-0.69 (2H, t, $-CH_2-$).

Immobilization of aromatic tertiary amine groups on the surface of attapulgite

Commercially available ATP contains densely packed fibrous clusters with small amounts of impurity, including quartz and carbonate. Therefore, before surface modification was carried out, the commercial ATP needed to be dissociated and purified. This can be achieved by pretreatment with 2% mass concentration of sodium hexametahposphate solution and 1 mol/L of hydrochloric acid respectively. The immobilization of aromatic tertiary amine groups was realized by self-assemble of aromatic tertiary amine coupling agent. A typical procedure was as follows, ATP (2.0 g) was dispersed in 150 mL toluene in a 250 mL three-necked round-bottom flask under ultrasonic vibration and strong stirring condition for 30 min. Then the synthetic SCA-ATA (4.0 g, 10.1 mmol) was added into the flask, and the immobilization was

carried out under reflux for 10 h. The solid product was separated by centrifugation, and washed several times with diethyl ether to remove absorbed coupling agent. The final solid product aromatic tertiary amine functionalized ATP (ATP-ATA) was dried in vacuum at room temperature.

RAFT polymerization of MMA using redox initiator

To a 25 mL Schlenk flask, aromatic tertiary amine groups anchored ATP (0.21 g, 9.4×10^{-5} mol) and methoxybenzene (2 mL, 1.84×10^{-2} mol) were added, and the mixture was ultrasonicated for 10 min to disperse particles homogeneously. BPO (22.8 mg, 9.4×10^{-5} mol), CPDB (17.5 μL, 9.4×10^{-5} mol) were dissolved in MMA (4 mL, 3.76×10^{-2} mol), and this solution was injected into the flask using a previously purged syringe. The flask was evacuated and back-filled with nitrogen three times, and then placed in oil bath at 50 °C for a prescribed time. After polymerization, the mixture was diluted with THF and centrifugated at 12000 rpm for 10 min, and the upper clean liquid was collected. The residue solid was washed several times with THF until there is no polymer in liquid. PMMA in all upper liquid was precipitated with excessive petroleum ether and collected by filtration. ATP grafted with PMMA hybrid particles (ATP@PMMA) and PMMA precipitated from liquid were dried at 50 °C in a vacuum oven for 24 h.

Cleaving grafted PMMA from particles

The grafted PMMA chains cleaved from the surface of ATP@PMMA via acidolysis of Schiff Base. About 100 mg of hybrid particles were dispersed in 5 mL hydrochloric acid (2 M) and 30 mL THF. The dispersion was allowed to stir at 80 °C

under ultrasonication for 24 h. the solvent was remove under vacuum, and the residual solid was dispersed in THF. The insoluble residue was separated by centrifugation, and PMMA solution was concentrated and recovered by adding excessive petroleum ether. The recovered PMMA was redissolved in anhydrous THF for GPC analysis.

Characterization

^{1}H NMR spectra was recorded by an Avance III 400 MHz Nuclear magnetic resonance spectrometer (NMR, Bruker, Switzerland) using $CDCl_3$ as a solvent and TMS as internal standard. Monomer conversion was recorded on an HP-6890 gas chromatograph (GC, Agilent, USA). Gel permeation chromatography (GPC) was performed on a Waters 515 GPC system equipped with three columns of average pore size 10^4 10^5, 10^6 nm and Waters RI detector at 35 ^{o}C. THF was used as eluent at a flow rate of 1.0 ml/min. Narrow molecular weight polystyrene (PS) standards were used for calibration of molecular weight and molecular weight distribution (M_w/M_n). Transmission electron microscopy (TEM) observations were conducted on a JEM-1200 EX/S transmission electron microscope with an accelerating voltage of 200 kV. The sample for TEM was prepared by placing 10 μL particles dispersion (0.2 g/L^{-1} in chloroform) on copper grids coated with a perforated carbon film. Ultraviolet and visible (UV-vis) absorption spectra were taken on a CARY-100 spectrophotometer. Fourier transform infrared (FTIR) were recorded on an Avatar 370 FT-IR spectrometer equipped with OMNIC software in the frequency range of 500-4000 cm^{-1}. The samples were prepared as KBr pellets and recorded by using a transmission mode at a resolution level of 2 cm^{-1}. X-ray photoelectron spectroscopy (XPS)

measurement was performed on a Thermo Fisher Escalab 250Xi spectrometer with a nonmonochromatic X-ray source (Al Kα radiation of 1361 eV). An electron flood gun was used to compensate for charging during XPS data acquisition. The step size was 1 eV (surveys) and 0.1 eV (region). X-ray diffraction (XRD) experiment was conducted at the scanning rate of 1°/minon using a Rigaku 18kw rotating anode X-ray generator with Cu Kα radiation operated at 40 kV and 100 mA. Corresponding data were collected from 5 to 60°. Thermo gravimetric analysis (TGA) was performed in nitrogen at a heating-up rate of 10 °C min^{-1} from 50 to 850 °C using a Netzsch TG209 F3 system. A sample weight of about 2 mg was used for all the measurements. The initiator grafting density (G_I) was determined by TGA using equation (1).[43] Where W_{ATP}% and $W_{ATP\text{-}ATA}$% were the percentage weight loss before and after surface functionalization between 50 and 850 °C, $M_{I\text{-}moiety}$ was the molecular weight of the silane moiety (265 for ATP-ATA). The weight (G_r), molar grafting ratio (G_p) of polymeric chains on ATP surface were determined by using the following equations (2) and (3) respectively.[44] Where $W_{ATP@PMMA}$% was the percent weight loss corresponding to the decomposition of ATP@PMMA, and $M_{n,GPC}$(g) was the number average molecular weight of grafted PMMA determined by GPC.

$$G_I = \frac{\frac{W_{ATP\text{-}ATA}\%}{100 - W_{ATP\text{-}ATA}\%} - \frac{W_{ATP}\%}{100 - W_{ATP}\%}}{M_{I\text{-}moiety}} \quad (1)$$

$$G_r = \frac{W_{ATP@PMMA}\%}{100 - W_{ATP@PMMA}\%} - \frac{W_{ATP\text{-}ATA}\%}{100 - W_{ATP\text{-}ATA}\%} \quad (2)$$

$$G_p = \frac{G_r}{M_{n,GPC}(g)} \quad (3)$$

Results and discussion

Synthetic pathway of ATP-supported organic/inorganic hybrid particles

ATP is a kind of hydrous porous magnesium aluminum silicate fibrillar mineral. It is abundant in nature with cheap price compared with the other nanomaterials. In terms of the nanostructure and low cost, ATP is a reasonable template to prepare rodlike organic-inorganic hybrid particles. Scheme 1 illustrates the synthetic pathway to prepare core-shell ATP@PMMA hybrid particles. Firstly, the surface modifier, SCA-ATA was synthesized via aldehydic-amide condensation catalyzed by PTSA. Then, ATP was treated with SCA-ATA using the alkyltrialkoxysilane groups as coupling point, and aromatic tertiary amine, which serves as the electron donor. During polymerization, the diethyl amino groups were firstly oxidated by BPO to generated azonia free radical. Subsequently, α carbon free radicals were formed by proton transfer, so high molecular weight of grafted polymer was achieved via SI-RAFT polymerization.

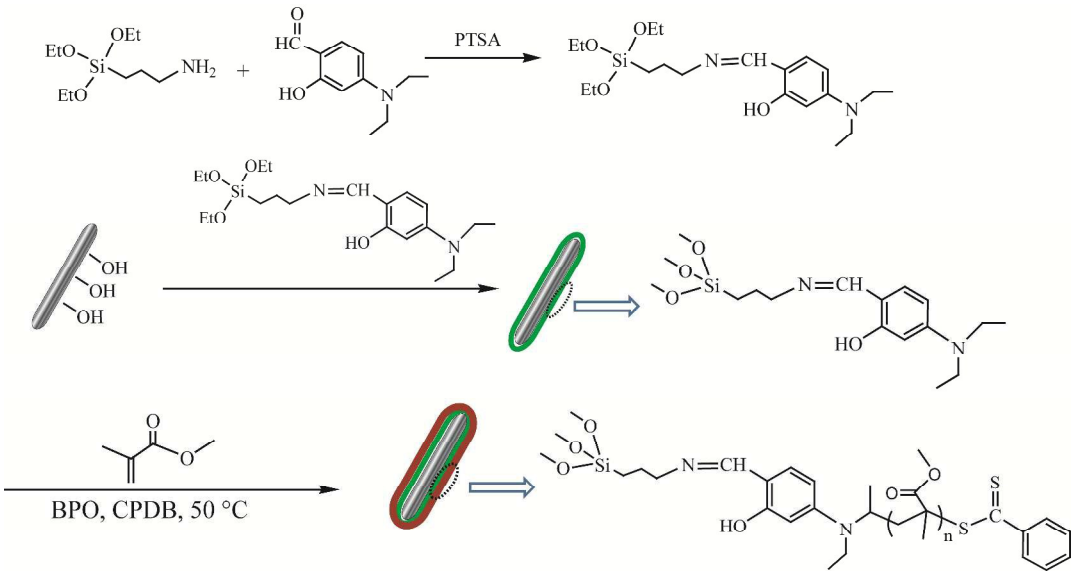

Scheme 1. Synthesis of ATP@PMMA via SI-RAFT initiated by redox initiation system.

Crystal structure and morphology of ATP@PMMA hybrid particles

The XRD patterns of ATP, ATP-ATA and ATP@PMMA are shown in Figure 1. It is found that there is no obvious difference among the scattering peaks, which demonstrates RAFT polymerization has no effect on the crystal structure of ATP. Natural ATP plays the role as a hard template and still exists in hybrid particles. Additionally, as a result of natural factors, the intergrowth-minerals of montmorillonite and quartz are also found in all patterns.

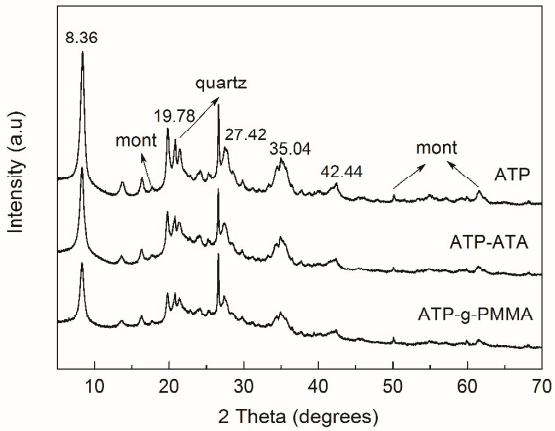

Figure 1. XRD patterns of ATP, ATP-ATA and ATP@PMMA.

As the inorganic core used in this work, typically TEM images confirm that ATP presents heavily agglomerate clusters with diameter of 20-40 nm of single nanorod (Figure 2a). The selected area electron diffraction (SAED) pattern consisting of light spots indicating the typical monocrystal structure of ATP (Figure 2b). It can be seen from Figure 2c that ATP@PMMA hybrid particles with discernible core-shell structure are formed after SI-RAFT, and the thickness of PMMA shell is attained to 18 nm with relatively uniform distribution. In Figure 2d, the SAED pattern of ATP@PMMA is similar with that of ATP except the relative intensity, which verifies

the resulted data based on XRD.

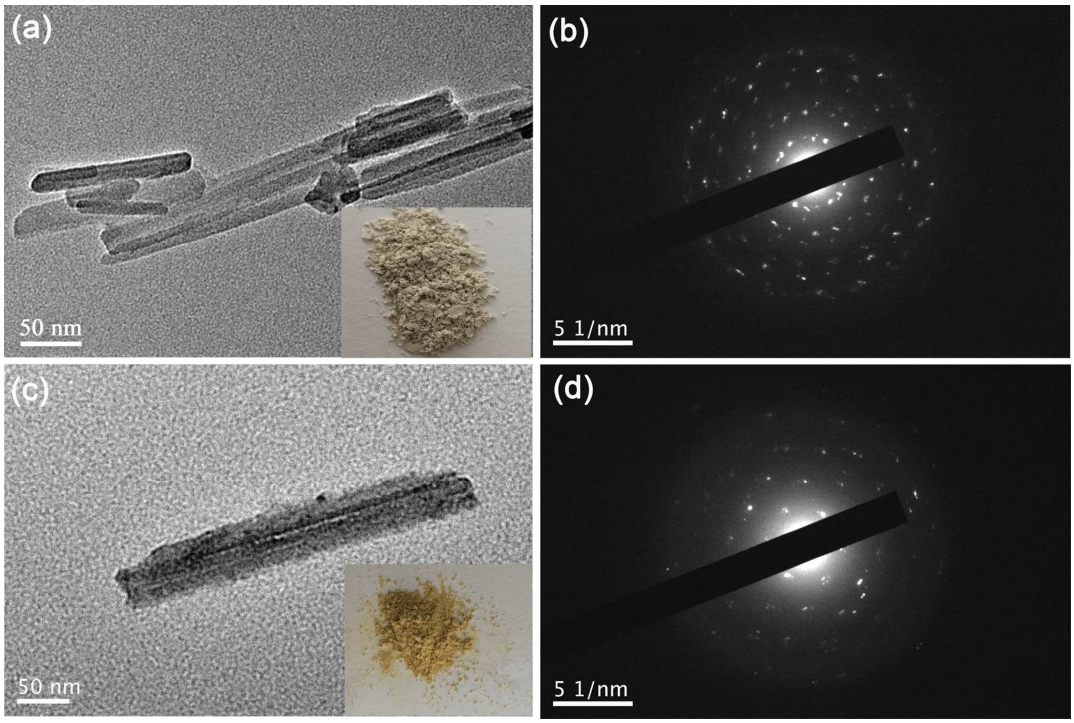

Figure 2. TEM images of (a) ATP and (c) ATP@PMMA, SAED patterns of (b) ATP and (d) ATP@PMMA.

Characterization of surface composition

Aromatic tertiary amine coupling with organic peroxides has been intensively investigated for radical polymerization of vinyl monomers containing electron withdrawing groups. Successfully grafting of PMMA on the surface of ATP was traced by UV-vis, FTIR, XPS, and TGA method. Figure 3 shows the UV-vis spectra of SCA-ATA, ATP and ATP-ATA. The SCA-ATA shows absorption at 215, 238 and 270 nm assigned to phenyl rings. The absorption at 363 nm is attributed to the C=N bonds. Scarcely any absorbance at visible region is found for bare ATP. After the attachment, ATP-ATA shows several new absorption bands that are similar to SCA-ATA, especially the obvious band of C=N groups. The absorption band at 356 nm in the spectra of ATP@PMMA prepared via RAFT polymerization is ascribed to

thiocarbonyl groups.[45]

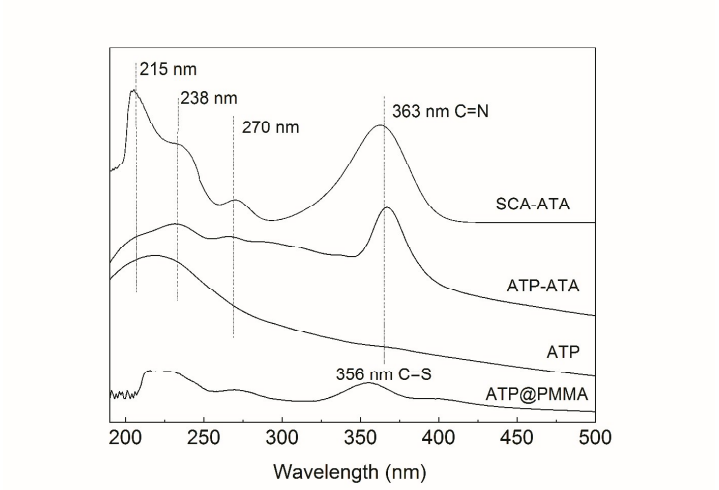

Figure 3. UV-vis spectra of SCA-ATA, ATP-ATA, ATP and ATP@PMMA.

The FTIR spectra of SCA-ATA, ATP, ATP-ATA and ATP@PMMA are presented in Figure 4. In the spectra of SCA-ATA, the peaks at 2973, 2929 and 2887 cm^{-1} are assigned to the stretching vibration of aliphatic C-H, and the absorption peaks at 824 and 785 cm^{-1} are attributed to aromatic C-H of 1,2,4-trisubstituted phenyl rings. The stretching vibration of Si-O-C gives two peaks at 1077 and 1126 cm^{-1}, and the characteristic peak at 1620 cm^{-1} is attributed to C=N of Schiff bass.[46] As for ATP, the two strong characteristic peaks at 984 and 1027 cm^{-1} are ascribed to the stretching vibration of Si-O-Si bonds of tetrahedral layers. Characteristic peaks for the abundant hydroxyl groups on the surface of ATP are founded at 1656 and 3550 cm^{-1} corresponding to the bending and stretching vibration respectively.[47] After ATP was functionalized with SCA-ATA, several new peaks, including 2974, 2931, and 1351 cm^{-1} bonds of C-H, 1519 cm^{-1} of aromatic ring skeletal, and the 1621 cm^{-1} of C=N groups, appear in the FTIR spectra of ATP-ATA. The spectra of ATP@PMMA presents a new strong peak at 1731 cm^{-1} assigned to the C=O stretching vibration of

ester group. Moreover, the peaks at 2995, 2951, 2855, 1386 and 1481 cm^{-1} attributed to alkyl chains are more intensive. The characteristic peak at 1518 cm^{-1} for phenyl ring still exists in hybrid particles, which maybe represent the terminal RAFT agents.

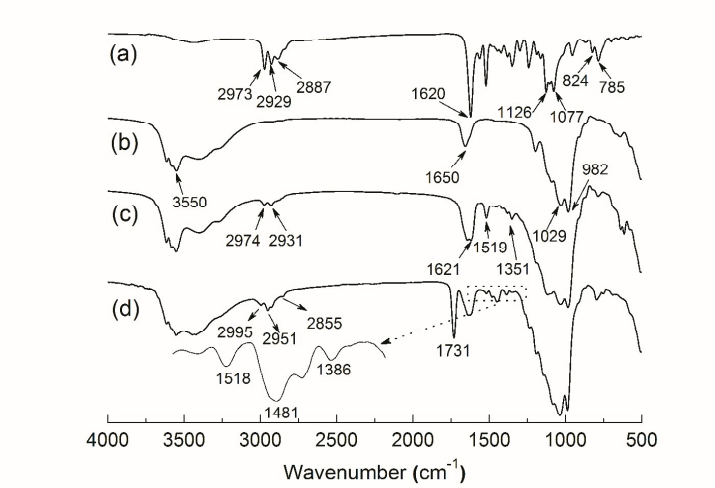

Figure 4. FTIR spectra of (a) SCA-ATA, (b) ATP, (c) ATP-ATA and (d) ATP@PMMA.

The surface chemical composition was further confirmed by XPS. The wide scan spectra of ATP (Figure 5a) is dominated by several signals at 103.3, 154.4, 284.8, 531.8 and 1304.4 eV attributable to Si2p, Si2s, C1s, O1s and Mg1s respectively.[48] These signals are corresponding to the formula of ATP. In the wide scan spectra of ATP-ATA (Figure 5b), a new peak of nitrogen (399.2 eV, N1s) is clearly observed. What's more, the signal intensity of Si2s, Si2p and C1s are increased significantly after surface modification. In Figure 5c, the C 1s and O1s peaks appeared around 285 and 532 eV with higher intensity are due to the considerably richer contents of these elements in PMMA. A weak S2p peak assigned to the sulfur element of RAFT agent is observed at 162 eV. The C1s core-level spectra of ATP-ATA (Figure 5d) can be curve-fitted into four peaks representing different carbons environment, 283.5, 284.7, 285.7 and 286.2 eV, attributable to C-Si, C-C/C=C/C-H, C-N and C=N/C-O

respectively.[49] The area ratio of the four peaks is close to 1:7:4:2 expected of SCA-ATA moiety. The C1s π-π* shake-up energy region of phenyl ring can be seen in the range from 289 to 296 eV. In the curve-fitted C1s spectra of ATP@PMMA (Figure 5e), five peaks with binding energy at 283.7, 284.7, 285.6, 286.5 and 288.6 eV are attributed to C-Si, C-C/C=C/C-H, *β*-shifted C1s of ester groups/C=S/C-N, C-O/C-S/C=N, and C=O, respectively.[50-52] All these results are the best evidence to confirm the successfully preparation of ATP@PMMA hybrids via SI-RAFT.

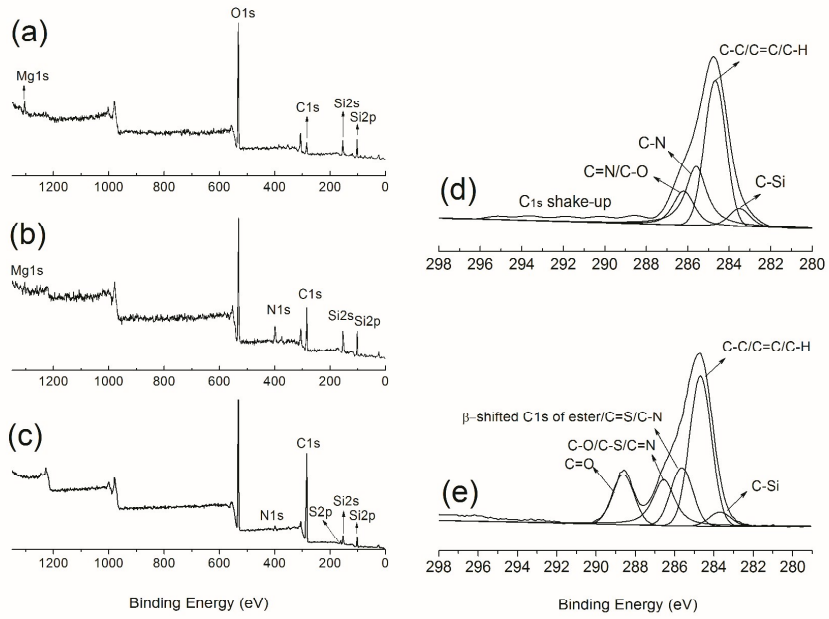

Figure 5. XPS wide scan spectrum of (a) ATP, (b) ATP-ATA, (c) ATP@PMMA, C1s core-level spectra of (d) ATP-ATA and (e) ATP@PMMA.

RAFT polymerization of MMA from the surface of ATP via redox initiation system

The grafting ratio of ATA groups and PMMA are quantitatively determined by TGA method. As shown in Figure 6, the weight loss of ATP below 150 ^{o}C and around 250 ^{o}C are attributed to the release of surface moisture and structural water. The

following weight loss after 250 ^{o}C corresponding to the zeolite water, crystal water and constitutional water, respectively. For ATP-ATA, the weight loss below 250 ^{o}C is similar to that of ATP, and the main degradation between 250 and 550 ^{o}C is assigned to the decomposition of surface organic components. The total weight loss for ATP and ATP-ATA are 10% and 18.3%. Consequently, we can roughly estimate that the loading amount of aromatic tertiary amine groups on the surface of ATP-ATA is 0.45 mmol/g calculated from equation (1). After grafting with PMMA, the weight loss of ATP@PMMA below 150 °C is decreased obviously, indicating that the surface hydrophilicity of ATP is alleviated. A significant weight loss is observed in the range of from 280 to 450 °C, which confirms the decomposition of grafted PMMA. The final weight loss of ATP@PMMA is 41.1%, and then the grafting ratio of PMMA relative to hybrids is calculated to be 47.4% by using equation (2). The molecular weight of grafted PMMA is 17723 g/mol as traced by GPC method, so the molar content (G_p) of PMMA in hybrid particles is estimated to be 26.7 μmol/g according to equation (3).

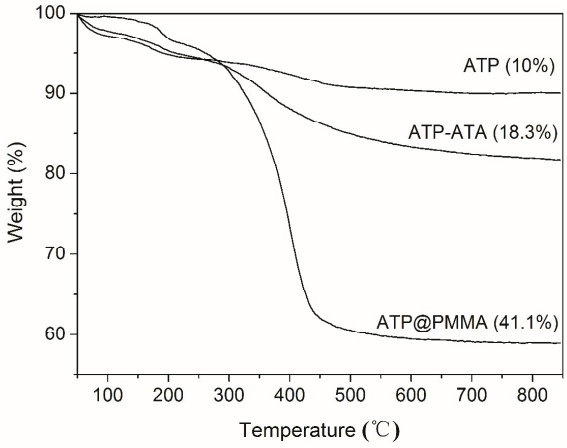

Figure 6. TGA curves of ATP, ATP-ATA, and ATP@PMMA.

The surface properties of particles both before and after grafting were examined by organic phase/water partitioning experiments. As seen from Figure 7, the hydrophobicity of ATP@PMMA is increased significantly after surface grafting. In the vial containing portion of water, MMA and10 mg of ATP@PMMA, it can be found that hybrid particles ATP@PMMA present a good dispersion in MMA and remain stable for a prolonged period. The grafted PMMA chains can prevent agglomeration, and thus dramatically increase the affinity to organic media.

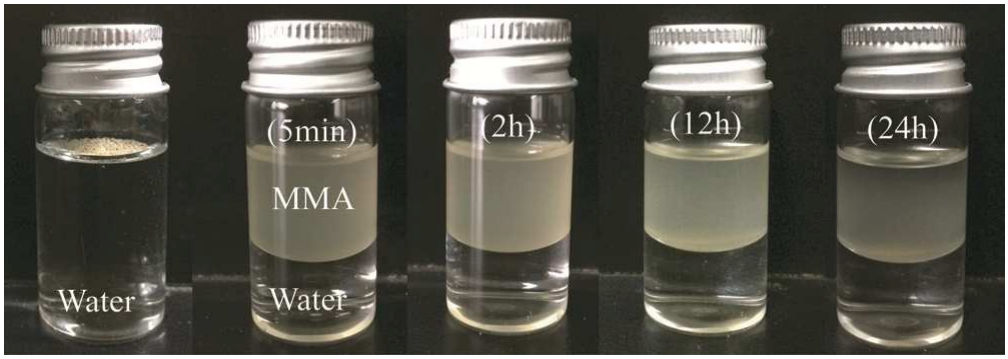

Figure 7. Image of organic phase/water partitioning experiments for ATP@PMMA.

In this system, CPDB mediated graft polymerization and homopolymerization simultaneously to maintain an efficient exchange reaction between dormant and active propagating species, and low polydispersity of both free and grafted polymer. As a redox initiation pair with dual active sites which generated grafted radicals on the surface and free radicals in solution simultaneously, there were a lot of free PMMA produced in solution in presence of free RAFT agent CPDB. According to our earlier research on RAFT-mediated "graft through" method on the surface of ATP, the surface grafting substantially depended on polymerization rate determined by the feed ratio of initiator of initiator and RAFT agent, as well as the polymerization temperature.[53] Hence, before the kinetic experiments, the effects of the above factors

were investigated. As shown in Table 1, it can be seen that the initiator and RAFT agent concentration impose the polymerization rate over the molecular weight, especially the grafting ratio of hybrid particles. Results show that faster or slower polymerization rate does not give the higher grating ratio owing to the unavoidable surface radical termination. When polymerization time was prolonged to 16 and 24 h under the condition of MMA/CPDB/BPO/ATA=400/1/1/1, the viscosity of reaction system increased substantially so that the constant stirring was unable to process. The obtained molecular weight dispersion value of grafted polymer was broadened (M_w/M_n> 1.4, Table 1 not shown). The possible reason is that surface-anchored active sites are generated at higher density, radical-radical termination could occur easily on individual particle or between two adjacent particles at higher conversion.[54] So, we used R.$_2$ to conduct the kinetic experiment, which can enhance the grafting ratio (47.4%) and keep the homogenous dispersion of reaction mixture (conversion 37.6%). As seen from Figure 8, a first-order kinetic plot for RAFT polymerization of MMA in presence of CPDB is maintained during the whole process, indicating the propagation radical concentration kept constant in the preseted polymerization time.

Table 1. Effect of initiator, chain transfer agent concentration, and polymerization temperature on RAFT polymerization of MMA

R[a]	Con.[b] (%)	$M_{n,th}$[c] (g/mol)	$M_{n,GPC}$(f)[d] (g/mol)	M_w/M_n[d]	$M_{n,GPC}$(g)[e] (g/mol)	M_w/M_n[e]	G_r[f] (%)	G_p[g] (μmol/g)
400/1/0.8/0.8	29.4	11981	14609	1.19	13098	1.23	23.4	16.8
400/1/1/1	37.6	15261	16021	1.2	17723	1.19	47.4	26.7
400/1/1.5/1.5	48.9	19729	18233	1.23	25659	1.31	14.2	5.6
400/1.5/1/1	31.8	8701	9716	1.18	12307	1.25	27.8.	22.5
400/2/1/1	27.3	5681	6830	1.15	7611	1.24	17.7	23.3
400/1/1/1	17.6	7271	9925	1.25	11156	1.19	12.1	10.9
400/1/1/1	52.9	21421	26808	1.21	30630	1.18	19.5	6.4

[a] R = MMA/CPDB/BPO/ATA, R.$_6$ and R.$_7$ were conducted at 40 and 60 °C respectively.

[b] Monomer conversion.

[c] $M_{n,th}$ = $[MMA]_0/[RAFT]_0$ × conversion × $M_{w,MMA}$ + $M_{w,RAFT}$, where $M_{w,MMA}$ and $M_{w,RAFT}$ represent the molecular weight of MMA and CPDB respectively, $[MMA]_0$ and $[RAFT]_0$ are the monomer mole number of MMA and RAFT agent at the beginning of polymerization.

[d] The molecular weight and its dispersion of free polymers measured by GPC.

[e] The molecular weight and its dispersion of grafted polymers measured by GPC.

[f] Weight content of grafted polymer related to hybrid particles measure by equations (2).

[g] Molar content of grafted polymer related to hybrid particles measured by equations (3).

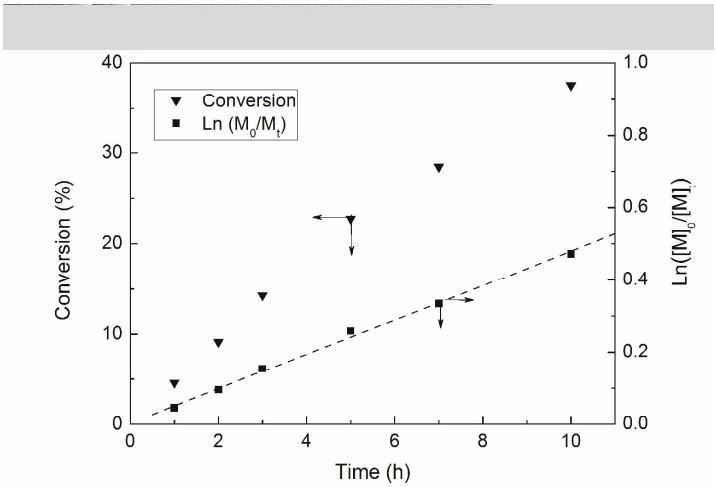

Figure 8. Monomer conversion and $Ln([M]_0/[M]_t)$ as a function of polymerization time for RAFT polymerization of MMA via redox initiation system at 50 °C. Polymerization conditions: MMA/CPDB/BPO/ATA = 400/1/1/1.

Figure 9 shows the evolution of the number-average molecular weight ($M_{n,GPC}$) and molecular distribution (M_w/M_n) value of the obtained cleaved polymer and free polymer simultaneously produced in solution with increasing monomer conversion. The $M_{n,GPC}$ value of both the grafted and free polymer increase linearly with monomer conversion while keeping low M_w/M_n (1.18-1.28). The experimental molecular weights of free polymer are close to the corresponding theoretical ones, and almost match the theoretical value especially in the case of high monomer conversions. The experimental results further confirm the "living" feature of this system. The M_n of grafted polymer was slightly higher than that of the free ones at high conversion (1.19-1.31), which is due to the surface radical-radical termination. As we can see in

Figure 10, the elution peak of grafted polymer chains shift to higher molecular weight with the increase of polymerization time, and has sharp and symmetric shape. All these results confirm that, CPDB mediated the surface graft polymerization and homopolymerization in solution simultaneously, and gave the controlled/LRP characteristics of RAFT polymerization.

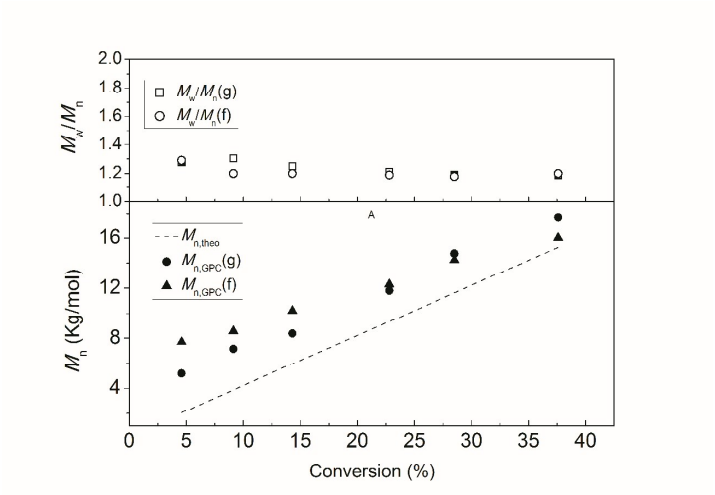

Figure 9. Evolution of number-average molecular weight and polydispersity index of grafted and free polymer as a function of monomer conversion for RAFT polymerization of MMA via redox initiation system at 50 °C. Polymerization conditions: MMA/CPDB/BPO/ATA = 400/1/1/1.

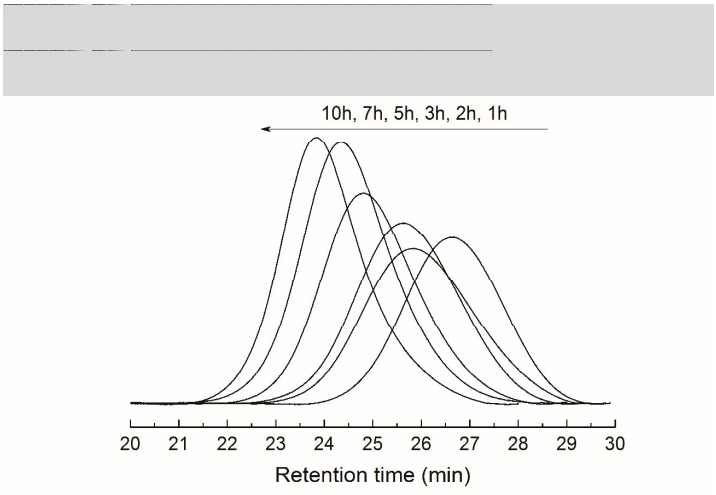

Figure 10. Evolution of GPC traces of the grafted polymers with polymerization time during RAFT polymerization of MMA via redox initiation system at 50 °C

Conclusion

The redox-initiated RAFT polymerization could be performed successfully by

using aromatic tertiary amine functionalized ATP coupled with BPO as the redox initiation pair in presence of free chain transfer agent. The successful grafting of PMMA on the surface of ATP was supported by UV-vis, FTIR, XPS, XRD, TGA and TEM data. Polymerization behavior presented the first order kinetic characteristic of controlled/living polymerization. The molecular weights increased linearly with monomer conversion and the corresponding polydispersities kept narrow for both the grafted and free PMMA. The grafted particles ATP@PMMA showed excellent dispersity in organic media, which is promising for the preparation of ATP nanocomposites and extending the application of ATP to other organic media-based field.

Acknowledgements

Financial support provided for this project by the Priority Academic Program Development of Jiangsu Higher Education Institutions (PAPD) is gratefully acknowledged.

REFERENCES

1 W. F. Bradley. *Am. Miner*., 1940, **25**, 405-410.

2 H. Zhang, W. C. Ye, F. Zhou. *J. Appl. Polym. Sci*., 2011, **122**, 2876-2883.

3 L. H. Xie, M. Z. Liu, B. L. Ni, Y. F. Wang. *Chem. Eng. J.*, 2011, **167**, 342-348.

4 D. L. Guerra, E. M. Silva, C. Airoldi. *Process*. *Saf*. *Environ*., 2010, **88**, 53-61.

5 L. Lu, X. Y. Li, X. Q. Liu, Z. M. Wang, L. B. Sun. *J*. *Mater*. *Chem*. *A*., 2015, **3**, 6998-7005.

6 L. F. Chen, H. W. Liang, Y. Lu, C. H. Cui, S. H. Yu. *Langmuir*, 2011, **27**,

8998-9004.

7 J. Gao, Q. Zhang, K. Wang, Q. Fu, Y. Chen, H. Y. Chen, H. Huang, J. M. Rego. *Compos. Part A*., 2012, **43**, 562-569.

8 Z. G. Qi, H. M. Ye, J. Xu, J. N. Chen, B. H. Guo. *Colloids. Surf A.*, 2013, **421**, 109-117.

9 R. G. Wang, Z. Li, Y. M. Wang, W. B. Liu, L. B. Deng, W. C. Jiao, F. Yang. *Polym. Compos.,* 2013, **34**, 22-31.

10 P. Liu, L. P. Jiang, L. X. Zhu, J. S. Guo. *J. Ind. Eng. Chem*., 2015, **23**, 188-193.

11 C. H. Liu, C. Y. Pan. *Polymer*, 2007, **48**, 3679-3685.

12 F. Zhou, W. T. S. Huck. *Phys. Chem. Chem. Phys*., 2006, **8**, 3815-3823.

13 T. Chen, R. Ferris, J. M. Zhang, R. E. Ducker, S. Zauscher. *Prog. Polym. Sci*., 2010, **35**, 94-112.

14 O. Azzaroni. *J. Polym. Sci. Part A: Polym. Chem.,* 2012, **50**, 3225-3258.

15 Z. Bogdan, L. Igor. *Macromol*. *Rapid*. *Commun*., 2011, **32**, 859-869.

16 F. J. Hua, E. Ruckenstein. *Macromolecules*, 2003, **36**, 9971-9978.

17 H. Roghani-Mamaqani. *RSC. Adv.*, 2015, **5**, 53357-53368.

18 C. M. Hui, J. Pietrasik, M. Schmitt, C. Mahoney, J. Choi, M. R. Bockstaller, K. Matyjaszewski. *Chem. Mater*., 2014, **26**, 745-762.

19 B. Wlodarczyk, R. Ferebee, M. R. Bockstaller, J. Pietrasik. *Polymer*, 2015, **72**, 348-355.

20 R. Jordan, A. Ulman. *J. Am. Chem. Soc*., 1998, **120**, 243-247.

21 R. Jordan, A. Ulman, J. F. Kang, M. Rafailovich, J. Sokolov. *J. Am. Chem. Soc*.,

1999, **121**, 1016-1022.

22 N. Zhang, S. Salzinger, F. Deubel, R. Jordan, B. Rieger. *J. Am. Chem. Soc*., 2012, **134**, 7333-7336.

23 T. V. Werne, T. E. Patten. *J. Am. Chem. Soc*., 1999, **121**, 7409-7410.

24 M. Nikdel, M. Salami-Kalajahi, M. S. Hosseini. *RSC. Adv*., 2014, **4**, 16743-16750.

25 M. Hatamzadeh, M. Jaymand. *RSC. Adv*., 2014, **4**, 28653-28663.

26 A. Bansal, A. Kumar, P. Kumar, S. Bojja, A. K. Chatterjee, S. S. Ray, S. L. Jain. *RSC. Adv*., 2015, **5**, 21189-21196.

27 B. S. Sumerlin, A. B. Lowe, P. A. Stroud, P. Zhang, M. W. Urban, C. L. McCormick. *Langmuir*, 2003, **19**, 5559-5562.

28 E. Pavoni, E. Bandini, M. Benaglia, J. K. Molloy, G. Bergamini, P. Ceroni, N. Armaroli. *Polym. Chem.* 2014, **5**, 6148-6150.

29 Y. Li, B. C. Benicewicz. *Macromolecules*, 2008, **41**, 7986-7992.

30 E. Zeinali, V. Haddadi-Asl, H. Roghani-Mamaqani. *RSC. Adv*., 2014, **4**, 31428-31442.

31 N. Zammarelli, M. Luksin, H. Raschke, R. Hergenröder, R. Weberskirch. *Langmuir*, 2013, **29**, 12834-12843.

32 Y. L. Zhao, S. Perrier. *Macromolecules*, 2006, **39**, 8603-8608.

33 L. P. Wang, Y. P. Wang, R. M. Wang, S. C. Zhang. *React. Funct. Polym*., 2008, **68**, 643-648.

34 M. H. Stenzel. *Maromol. Rapid. Commun*., 2009, **30**, 1603-1624.

35 M. Baum, W. Brittain. *Macromolecules*, 2002, **35**, 610-615.

36 S. Demirci, T. Caykara. *React. Funct. Polym*., 2012, **72**, 588-595.

37 A. S. Sarac. *Prog. Polym. Sci*., 1999, **24**, 1149-1204.

38 H. T. Zheng, W. Bai, K. L. Hu, R. K. Bai, C. Y. Pan. *J. Polym. Sci. Part A: Polym. Chem*., 2008, **46**, 2575-2580.

39 A. Sanchez-Sanchez, I. Asenjo-Sanz, L. Buruaga, J. A. Pomposo. *Maromol. Rapid. Commum*., 2012, **33**, 1262-1267.

40 W. Bai, L. Zhang, R. K. Bai, G. Z. Zhang. *Maromol. Rapid. Commun*., 2008, **29**, 562-566.

41 J. Chiefari, Y. K. Chong, F. Ercole, J. Krstina, J. Jeffery, T. P. T. Le, R. T. A. Mayadunne, G. F. Meijs, C. L. Moad, G. Moad, E. Rizzardo, S. H. Thang. *Macromolecules*, 1998, **31**, 5559-5562.

42 H. C. Yang, L. Zhang, W. Z. Ma, H. T. Pu, F. H. Gong. *J. Appl. Polym. Sci*., 2015, **132**, DOI: 10.1002/app.41567.

43 M. Save, G. Granvorka, J. Bernard, B. Charleux, C. Boissière, D. Grosso, C. Sanchez. *Macromol. Rapid. Commun*., 2006, **27**, 393-398.

44 T. Y. Guo, P. Liu, J. W. Zhu, M. D. Song, B. H. Zhang. *Biomacromolecules*, 2006, **7**, 1196-1202.

45 J. L. Liu, L. F. Zhang, S. P. Shi, S. Chen, N. C. Zhou, Z. B. Zhang. *Langmuir*, 2010, **26**, 14806-14813.

46 R. M. Issa, A. M. Khedr, H. Rizk. *J. Chin. Chem. Soc*., 2008, **55**, 875-884.

47 Y. Kong, J. Yuan, Z. L. Wang, S. P. Yao, Z. D. Chen. *Appl. Clay. Sci.*, 2009, **46**,

358-362.

48 P. Liu. *Appl. Clay. Sci*., 2007, **35**, 11-16.

49 F. Truica-Marasescu, M. R. Wertheimer. *Plasma*. *Process*. *Polym*., **2008**, 5, 44-57.

50 L. B. Feng, L. He, Y. X. Ma, Y. L. Wang. *Mater. Chem. Phys*., 2009, **116**, 158-163.

51 C. Zhou, S. S. Qian, A. K. Zhang, L. Q. Xu, J. Zhu, Z. P. Cheng, E. T. Kang, F. Yao, G. D. Fu. *RSC. Adv*., 2014, **4**, 8144-8156.

52 S. P. Shi, L. F. Zhang, J. Zhu, W. Zhang, Z. P. Cheng, X. L. Zhu. *Express. Polym. Lett*., 2009, 3, 401-412.

53 L. Zhang, H. C. Yang, Q, T. Ni, H. Liu, Y. Chen, F. H. Gong. *Acta. Polym. Sin.,* 2014, **58**, 400-405 *(in chinese).*

54 Q. Li, L. F. Zhang, Z. B. Zhang, N. C. Zhou, Z. P. Cheng, X. L. Zhu. *J. Polym. Sci. Part A: Polym. Chem*., 2010, **48**, 2006-2015.

Table of contents entry

Polymethyl methacrylate layer was grown uniformly from attapulgite by using surface-initiated reversible addition-fragmentation chain transfer polymerization via redox initiation system.